

# Simulation and Flight Test of a Temperature Sensing Stabilisation System

P. Herrmann                      C. Bil                      S. Watkins                      B. Taylor  
Sir Lawrence Wackett Centre for Aerospace Design Technology  
School of Aerospace, Mechanical and Manufacturing Engineering  
RMIT University  
Melbourne  
AUSTRALIA

## ABSTRACT

Thermopile sensors read electromagnetic radiation as a function of the object's temperature. Because there is a temperature difference between the cold ground and the warm sky, these sensors could be used to detect the horizon and thus be used as a reference to stabilise a small aircraft, such as a UAV. To verify this hypothesis, a system has been developed that uses horizon detection using thermopile sensors to stabilise an R/C aircraft model. The aircraft has gone through a number of flight trials using remote control to enable and disable the stabilisation system. During the flight trials the aircraft was given various bank angles when the system was enabled. The stabilisation system was able to assume wing level under various bank angles and weather conditions with minimum overshoot and oscillation.

Although the system shows good performance during flight trials, most of the design was done using trial and error. A design tool was needed to implement further improvements to the system and to efficiently implement it on other aircraft. This required a good understanding of the physical behaviour of the system and the interaction between the sensors, aircraft and the environment. A mathematical overall system model was developed and the MATLAB/Simulink toolbox was used to simulate the behaviour of the system under various conditions. The simulation results were then compared with actual flight experiments. This paper describes the modelling techniques used for the different system components and the results of the simulation compared to actual flight trials.

## BIOGRAPHY

Paul Herrmann is a graduate computational engineer at VPAC (Victorian Partnership of Advanced Computing), having graduated with from a bachelor degree in Aerospace Engineering and Applied Science (Aviation) in 2003. He is involved in several ongoing UAV projects including a low cost inertial reference system for commercial UAV's.

Cees Bil graduated from Delft University of Technology and was assistant professor at the Faculty of Aerospace Engineering until 1995. In 1995, he joined the Department of Aerospace Engineering at RMIT University where he leads the research in aerospace design. He is a member of the ICAS Program Committee and vice chairman of the Royal Aeronautical Society Melbourne Branch.

Simon Watkins graduated from Bristol University and worked for British Aerospace before undertaking aerodynamic research for magnetically levitated trains at City University, London. Since 1983 he has worked at RMIT, including work on drag reduction of commercial vehicles and trains and on car aerodynamics and aeroacoustics. He is chair of the Vehicle Aerodynamics Forum and the Wind Noise Subcommittee of the International Society of Automotive Engineers.

Brian Taylor is an electronics engineer studying for a Masters Degree at RMIT University. He is an Honorary Research Associate at Monash University, currently developing a low cost UAV for civil applications based on his design for a Horizon Sensing Attitude Stabiliser and GPS tracking software.

**Atmospheric temperature sensing – background**

All matter emits electromagnetic radiation as a function of its temperature. In this application thermopile sensors are used to distinguish the relatively cold sky from the warm ground. A sensing system incorporating thermopiles was designed, built and tested on a model aircraft to detect the horizon and use it as a reference to stabilise the aircraft. This technique offers a low-cost solution for the stability and control on model aircraft and UAVs.

Thermopiles are essentially a micro array of dissimilar metal junctions with hundreds of very thin, thermally isolated ‘hot junctions’ exposed to incoming radiation and the ‘cold junctions’ thermally bonded to the sensor case. A silicon IR filter restricts the incoming radiation to a narrow band of the IR spectrum (8-14µm). This band is selected for sensitivity to blackbody radiation from objects with a temperature in the range between -75° C to 75° C. Conveniently, the Earth’s atmosphere provides good transmission in this narrow range. See Taylor<sup>8</sup> for a more complete description.

**Thermopile sensor specifications**

Figure 1 shows the technical details of the thermopiles used, including a functional diagram of the thermopile sensor. Note that NTC temperature sensor is not used, as the absolute temperature is not required, only the differential of the pair of sensors, which are in series, arranged ‘back to back’. This assumes that the case temperature of both sensors is the same.

|                                      |                   |
|--------------------------------------|-------------------|
| Manufacturer / Model No.             | Melexis 90247 DSE |
| Sensitivity (µV/degK)<br>min/typ/max | 29 / 40 / 55      |
| Package                              | TO-39             |

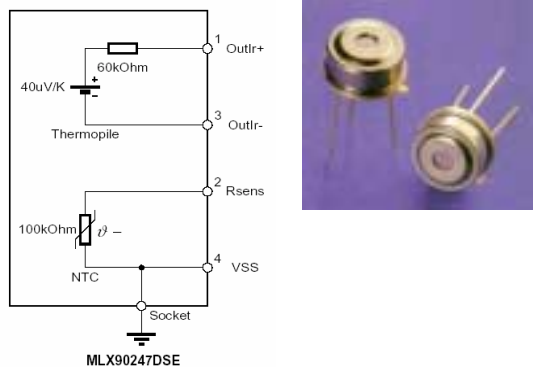


**Figure 1: Melexis 90247 Thermopile Sensors Specifications.**

**Atmospheric thermal modelling**

In order to model and evaluate the performance of this guidance system, we first need to gain some insight into the thermal signal radiated from the environment around the aircraft. As thermopile sensors are commonly employed in non-contact thermometers, the use of such a device provided a simple method of obtaining temperature data in a variety of atmospheric conditions. The unit used (Raytek MT-2 Minitemp) had a field of view of 20°, substantially narrower than the naked Melexis sensors being used in the autopilot system; these are believed to provide a square field of view (FOV) of 100°. Note that these sensors are less sensitive than those in the Raytek to fine detail because any thermal irregularity will occupy a smaller portion of the FOV.

The readings shown in Figure 2 are for a single sensor producing an absolute temperate value. The ground temperature is relatively warm in comparison to the cold sky, which may read as low as -30°C in clear (no cloud or precipitation) conditions. This trend is the fundamental concept that is to be exploited to provide attitude control. The autopilot sensors comprise of a differential pair of sensors about two axes (pitch and roll). As no suitable hardware was available at the time of testing, the sensor pair was simulated by assuming that the atmospheric temperature distribution is symmetric about the vertical plane. By observing the above assumption, the data was normalised with respect to the minimum/maximum (sky/ground) temperatures, and the results are shown in Figure 3.

Of the sample data shown, four plots behave in an expected and repeatable manner. The region of greatest change occurs near the horizon providing the highest sensitivity. The remaining three readings (F-2, F-6 and F-7) show sensor response under different adverse conditions. F-2 - is typical of the effect of high, patchy cloud cover. The performance within ±30° of the horizon is generally good, but the influence of the warm clouds (5°C Approx) present above 40° from the horizon cause the differential measurement to be lower than under clear conditions. Given that the control gain is derived from the maximum sky-to-ground temperature differential, such conditions generate an artificially high gain. This is visible on the normalised plot as regions where the value exceeds the bounds of 1 and -1.

F-7 - is also the result of patchy cloud cover, this time extending from the horizon (180°) to 220°. Since the gain is based on the clear sky reading, it will be lower than optimal at angles where clouds are visible.

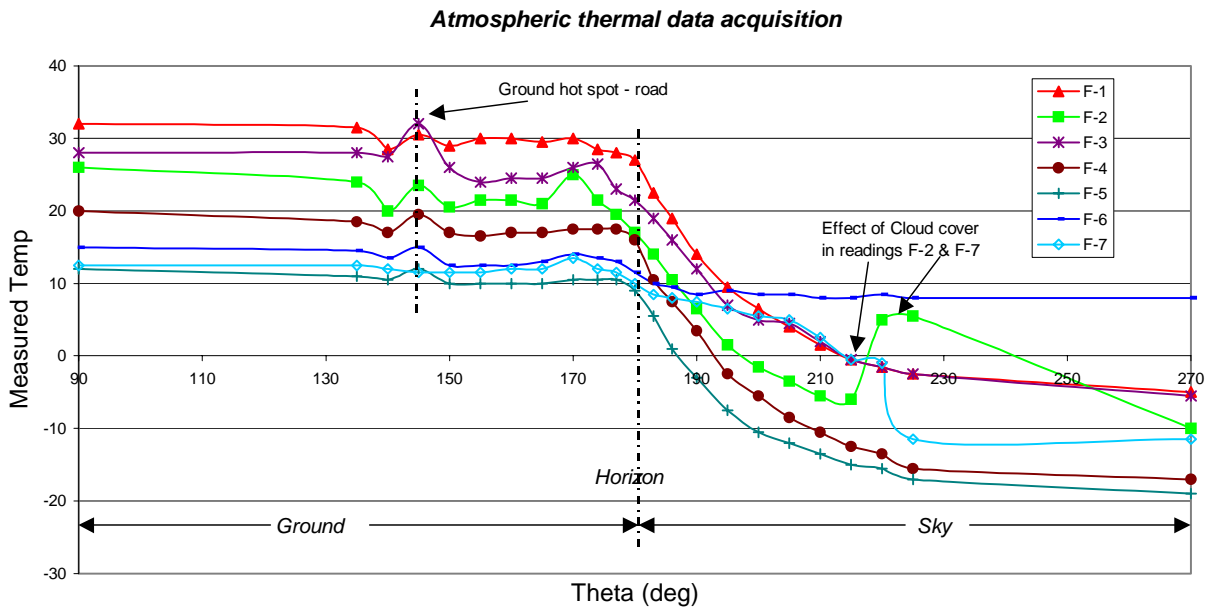


**Figure 2: Plots of temperature vs azimuthal angle for a series of recordings under differing weather conditions.**

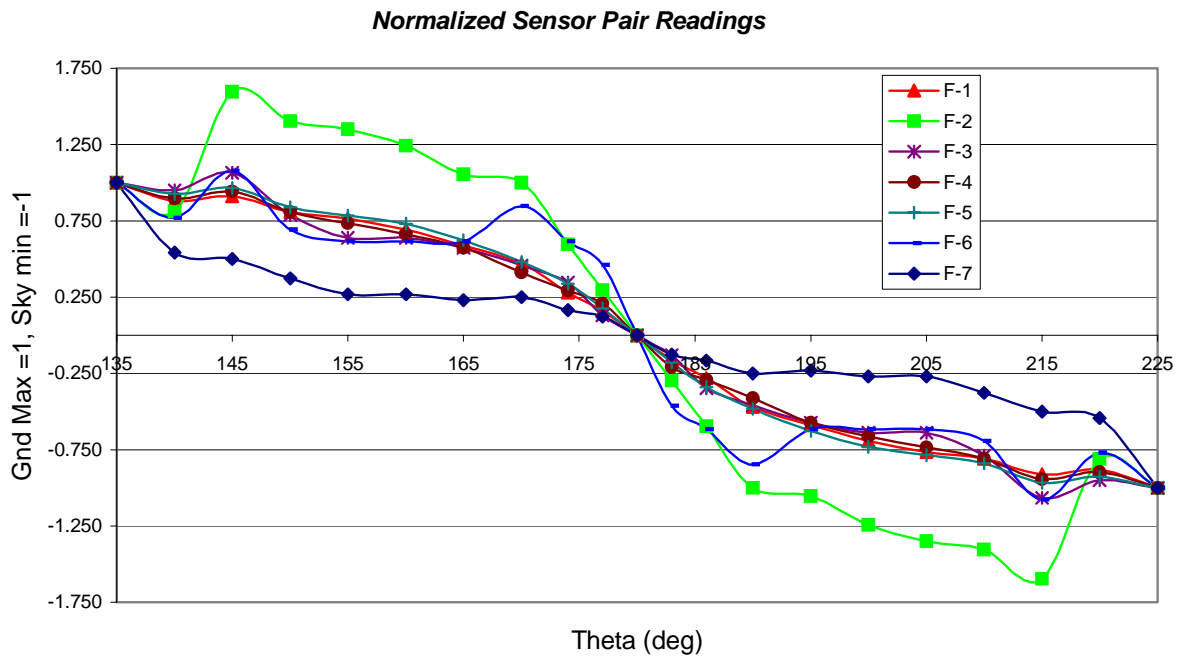


**Figure 3: Normalized sensor pair readings derived from Figure 2 data.**

F-6 - this reading shows the normalised response under overcast low cloud cover. In this case the maximum differential temperature is reduced to only 7°C. (4°C Was the smallest observed during testing, 20-30°C is typical in clear conditions.) 'Noise' is apparent here as small variations in sky and surface temperature have a relatively large influence given the high gain associated with this small maximum differential temperature.

Analysis of these atmospheric thermal measurements highlights several challenges & potential pitfalls of such a system. Degraded performance would be expected in cases of very low maximum temperature differential (MTD). Two factors are important here, the actual measurement resolution of the system and the impact of hot or cold spots appearing within the sensor. The prototype system has flown successfully in hazy conditions where the MTD was only 3°C. Safe operation inside dense cloud is not expected due to the MTD being virtually zero in these instances. However, operation between bands of cloud is expected to be possible due to the adiabatic lapse rate causing a measurable temperature differential between cloud layers. Note that the averaging effect of having a wider FOV will allow the actual system to cope better with irregular cloud coverage and ground based 'hot spots' than these tests results indicate. This integration or averaging effect of the source field within the FOV is addressed in the simulation.

In order to model the controller behaviour in varying atmospheric conditions, a generic atmosphere temperature model was created, simulating the sensor pair response. The approach was to build a model representing the temperature around 360 degrees of rotation (roll or pitch). Based on the previously examined test data and taking into account the field of view that the Raytek (see previous section) unit had, the following model was constructed in Maple. It consists of three discontinuous heviside functions, two sinusoids representing 160° of ground and sky respectively and a cubic spline fitted between the remaining 20° at each horizon, joining the two sinusoids together. The original approach was that four temperatures could be specified (Ground max and min, Sky max and min) as indicated below. Since the temperature measurement is differential this model has only two independent inputs. The approach was then to perform definite integration over a range of 100°, representing the viewing angle of the thermopiles. The mid point of this integration range represents the orientation of the sensor and the integral divided by the viewing angle is the measured temperature. This process was conducted in a loop to calculate the response of the sensor pair around a

complete revolution. This output was left in terms of the defining temperatures (Ground max and min) and exported as a matrix, forming a lookup table within the dynamic Simulink model. This approach added negligible computation time to the dynamic model, while allowing realistic sensor performance to be simulated.

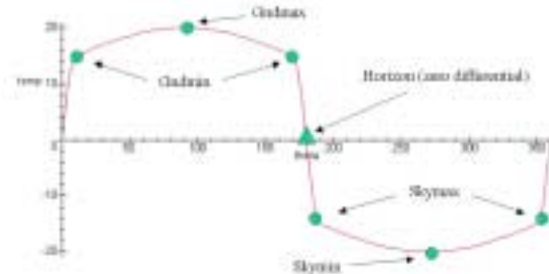


**Figure 4: Atmospheric temperature model representing one axis (pitch or roll). Note that 180° and 360° represent the horizon in each direction.**

As the field of view of the thermopile sensing elements is square (100° in each direction) an 'influence function' was incorporated in the above integration process. This allows for the orientation of the sensing elements with respect to the horizon. It is assumed that each sensor is aligned with its differential pair. A series of these influence functions are shown in figure 5, for a range of sensor rotation angles from 0° to 45°. For example, if the pitch angle of the aircraft is zero, then the roll influence function is constant throughout the sensors' field of view, represented by the cyan square in Figure 5 ( $\phi = 0^\circ$ ). If the aircraft were now to pitch 45° nose up, the sensitivity of the roll sensor would now be altered such that the pink triangle represents its effective field of view ( $\phi = 45^\circ$ ).

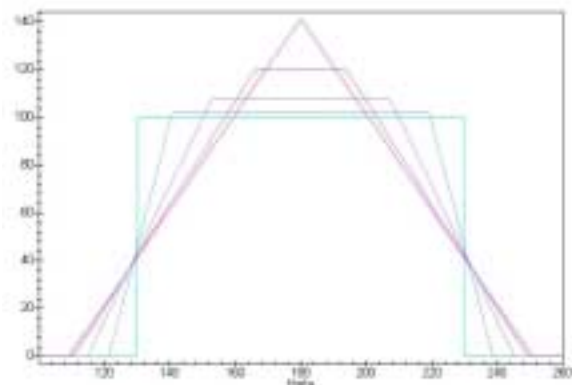


**Figure 5: Influence functions for a range of sensor rotation angles ( $\phi$ ).**

This method is strictly valid for small angles, since at larger angles one axis will affect the sensitivity of the other. In an extreme case, for example nose pitch up 90°, the sensitivity of the roll axis is now

zero since the roll sensor pair will ‘see’ the horizon regardless of their position ( $\phi$ ). This is only a limitation of the current model and does not imply that the real controller cannot function in these extreme orientations.

It was ultimately found that the sensor response was only marginally affected by the orientation of the sensor pair. This is illustrated in figure six which shows that rotation of the sensor away from zero results in a reduction of effective gain of up to 8% at 45°. Zero rotation is defined when two of the sides of the square field of view are parallel with the horizon. It does remain important that each differential pair is orientated correctly to prevent the controller behaving differently when rolled or pitched each way from the trim position.

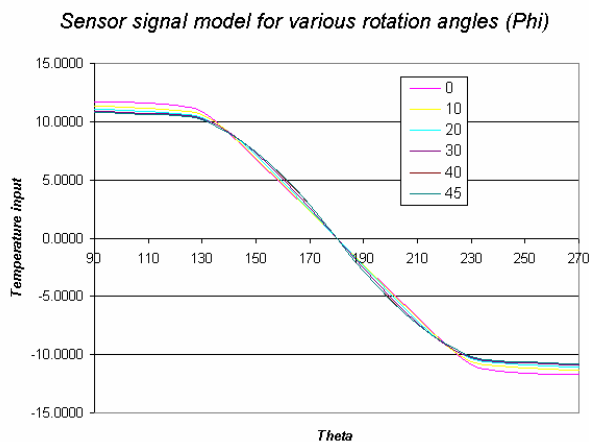


**Figure 6: Sensor response vs. rotation angles  $\phi$ .**

### Aircraft Modelling

For any dynamic model aircraft model to provide useful results, both the inertial characteristics and aerodynamic derivatives must be known or approximated. Given the apparent complexity of finding the moments of inertia by experiment (swinging the aircraft as a pendulum) [1,2], a solid CAD (CATIA) model was produced of the test-bed aircraft (Figure 7). It was envisaged that this approach would require less time, but also has two main advantages over the experimental option. Firstly, CATIA will also calculate the products of inertia (one of which is used in the Aerosim inertial model) and secondly, this approach lends itself to modification of the airframe. The next intended variant would have the prop mounted higher allowing the inclusion of a rotating nose cone.

The aerodynamic derivatives can be measured experimentally through instrumented flights or wind tunnel testing. Alternatively, a basic estimation can be made from analysis of similar aircraft. In this case modified parameters for the Cessna C-172,

supplied with the Aerosim toolset were used since the test aircraft is the same basic configuration and geometrically similar. This is a simplification, but allowed project time to be devoted to more core activities such as sensor modelling. Any further work on this project should aim to better understand the aerodynamic performance and derivatives of the test aircraft. A digital model of the aircraft was created.



**Figure 7: Trainer model used in flight tests (wingspan = 1.6 m).**

Each sub-assembly was generated from measurements of the test aircraft; Density was applied to produce the correct component and total weights. The CG location, moments and product of Inertia  $I_{xx}$ ,  $I_{yy}$ ,  $I_{zz}$  and  $I_{xy}$  are then imported into a MATLAB configuration script which defines the aircraft parameters to be used for simulation.

### Aerosim – Dynamic Aircraft Model

Figure 8 provides an overview of the Simulink model; the segments labelled 1-6 are as follows.

- 1) Aerosim 6-DOF Dynamic aircraft model
- 2) Aircraft state output, plotting & data logging
- 3) Atmospheric input parameters (Ground-Sky, Max and min) and sensor self calibration
- 4) PID feedback controller – pitch and roll
- 5) Pitch and roll thermopile based sensors (analogue)
- 6) Digital processing and delay

The simulation is commenced aircraft in a user-defined state (attitude, roll and pitch rates, airspeed etc) and run at a fixed time step, typically 0.02sec (50hz). At each time step, the aircraft attitude is fed into to the atmosphere/thermopile model. The digital processing of the autopilot and resultant delays

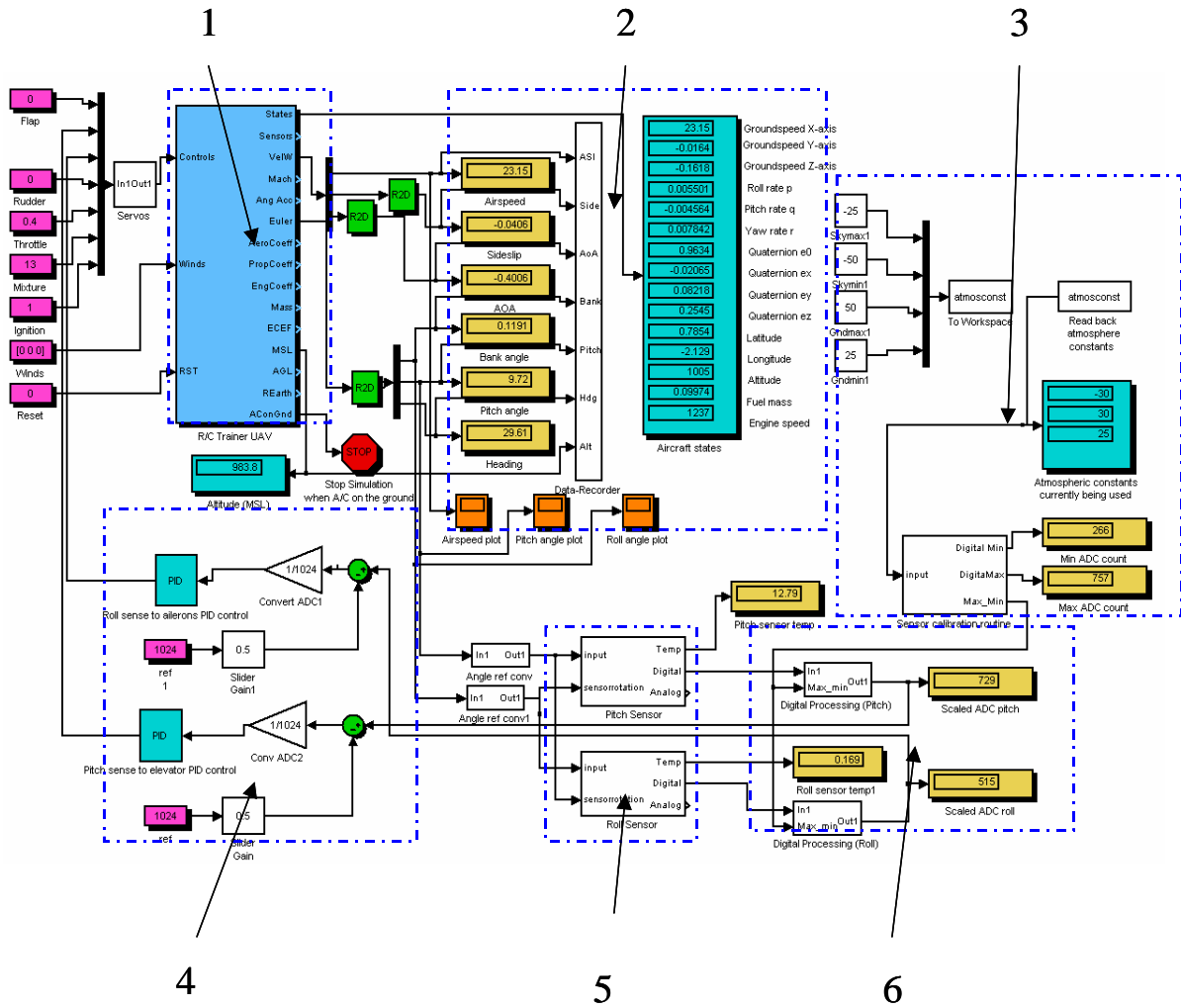


**Figure 8: Simulink model incorporating sensor feedback control of the dynamic aircraft model.**

is simulated, with the output of the PID controller driving the servos – this completes the plant-control loop. The resultant aircraft motion is displayed during the simulation, and is also stored for later analysis.

Figure 9 shows a schematic of the Aerosim 6-DOF Dynamic aircraft model. This module is provided as part of the Aerosim package from [7], it forms the heart of the dynamic simulation. All the relevant aircraft parameters are read from a MATLAB \*.mat file prior to the simulation run allowing for simple alteration of aircraft set-up or simulation of an entirely different aircraft utilising the same guidance system.

Figure 11 shows the calibration routine; simulating the pre-flight calibration of the aircraft, where the minimum and maximum temperatures (sky and ground) are converted into ADC (analogue-to-digital converter) counts. Outputs 1 and 2 display these values to the user; output 3 transfers these values to the digital processing segment – segment 6. Note that the thermopile element in figure 12 is itself a two-dimensional lookup table for each axis,

craft orientation and atmospheric variables provided in segment 3 (see model overview). This allows simulation of sensor rotation ( $\phi$ ) as described previously.

Figure 13 shows the digital processing and delay segment. This segment is used to simulate the 8-bit micro-controller used to process the sensor data and generate the PID control loops. It essentially models the loss of precision through rounding and a delay representing the code execution time. The servos from the Simulink block-set allow input and output saturation limits, maximum rate and bandwidth of the actuators to be modelled. Given that the thermopile sensor bandwidth is approximately 30hz, the servos and coupled control surfaces represent the major latency in the system, and thus the limitation for the maximum allowable controller gains for which the system is stable. The following parameters were used to model the servo actuators.

- Max rate: 1.5 rad/sec (86 deg/sec)
- Bandwidth: 10 Hz

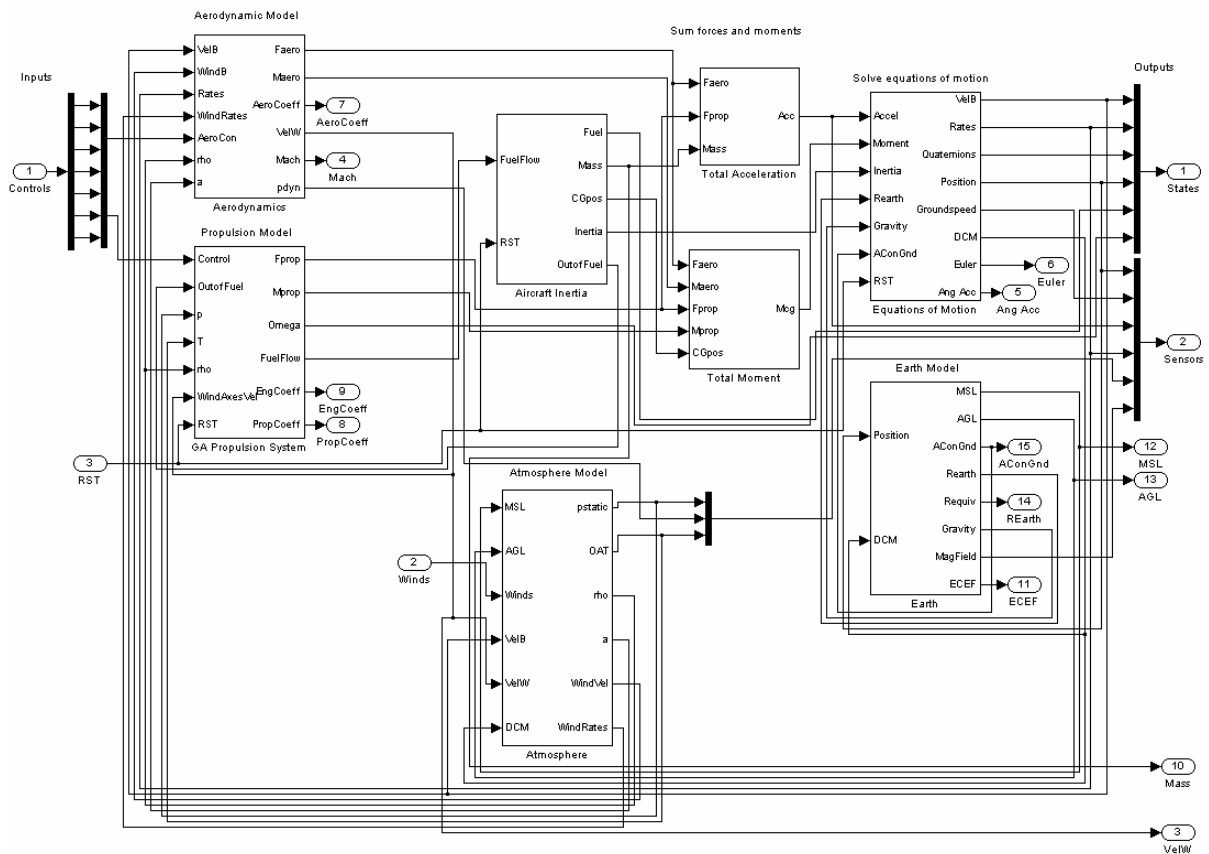


Figure 9: Inside the Aerosim 6-DOF aircraft model – Segment 1

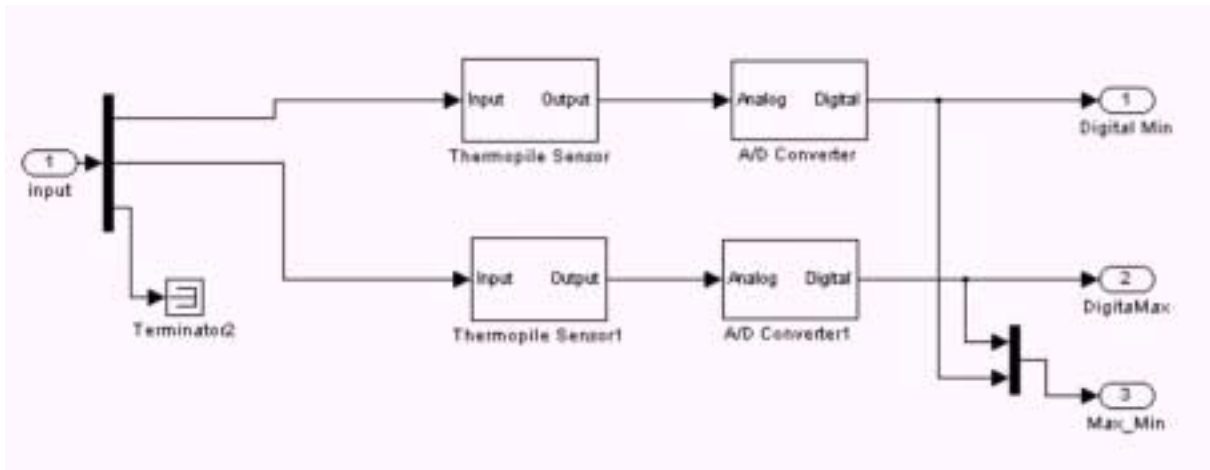


Figure 10: Thermopile sensor calibration to current atmospheric conditions – Segment 3.

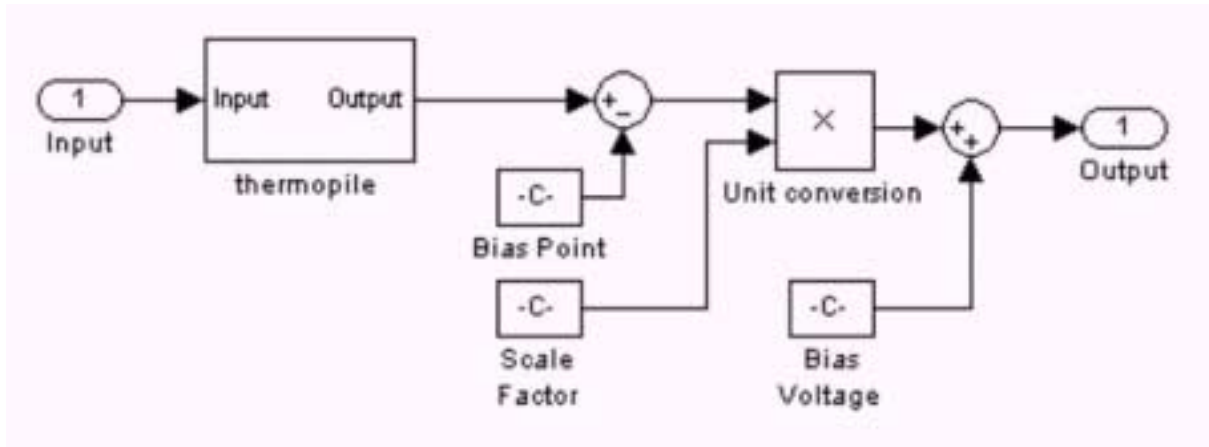


Figure 11: Thermopile analogue processing – zero offset and scale – Segment 5

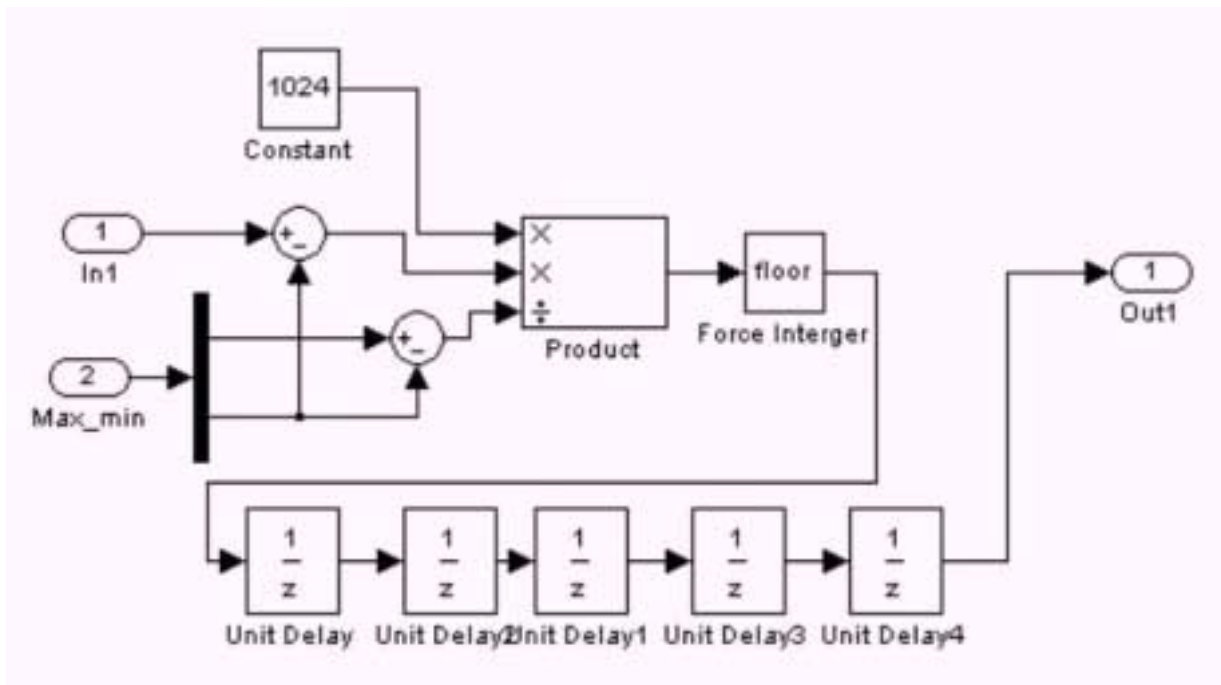


Figure 12: Digital processing and delay – Segment 6.

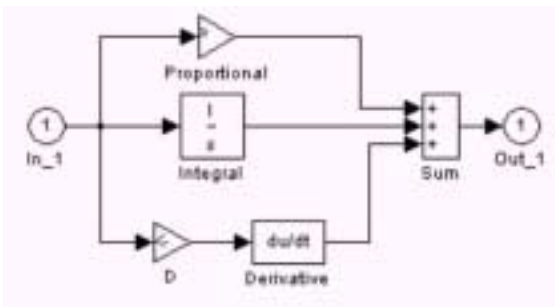


Figure 13: PID (Proportional, Integral and Derivative) control loop – Segment 4

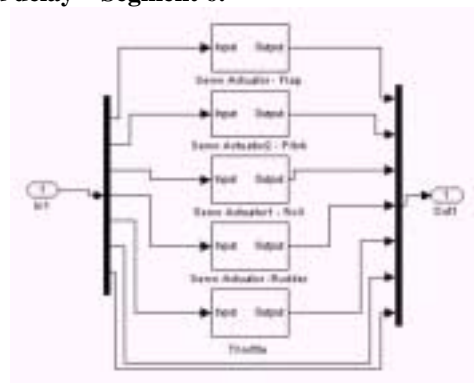


Figure 14: Control servo block – as shown to the left of segment 1



### Results

As a test of the ability of the simulation's accuracy, the following manoeuvre was performed during flight-testing; from steady state, straight and level flight, a manual snap roll is performed by the remote control pilot, at the instance of reaching 90° (such that the wings are now vertical) the autopilot is engaged and manual control ceases. The flight test was captured on digital video and later analysed using the VideoPoint frame capture software [9]. The aircraft response is plotted in Figures 15

and 16 from the instance of autopilot engagement. The three curves show the repeatability of the test procedure. Note that the pitch-roll interaction during this manoeuvre was minimal and was ignored principally because of the limitations of this test procedure. Any further flight-test validation would benefit greatly from the use of on-board instrumentation to accurately record the aircraft's dynamic response.

### Experimental Results of 90 degree roll recovery

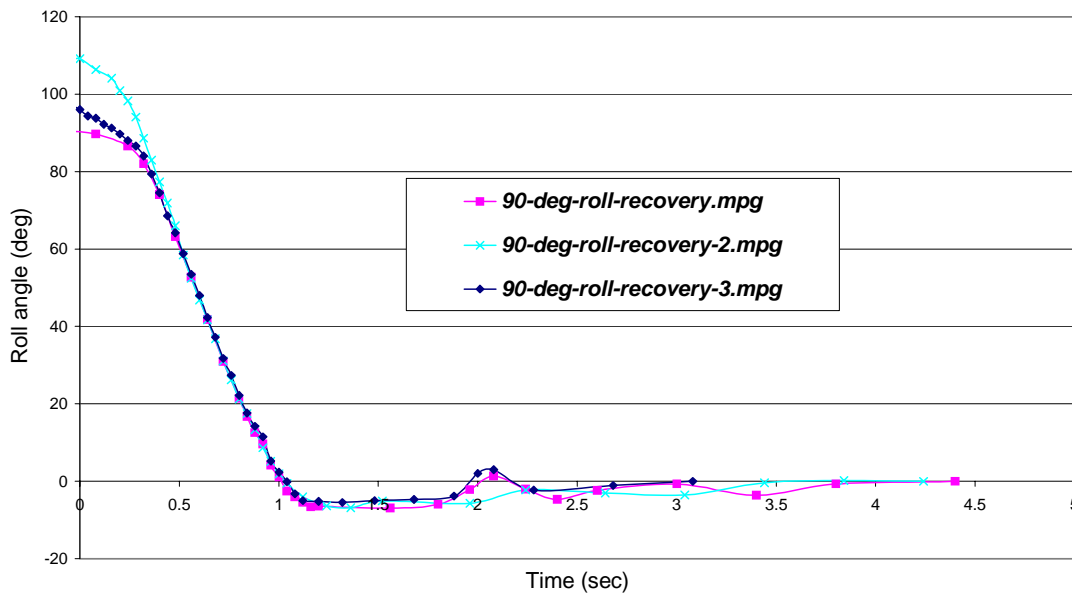


Figure 15: Flight test results of 90 degrees roll recovery.

### Comparison of Experimental & Simulated Results

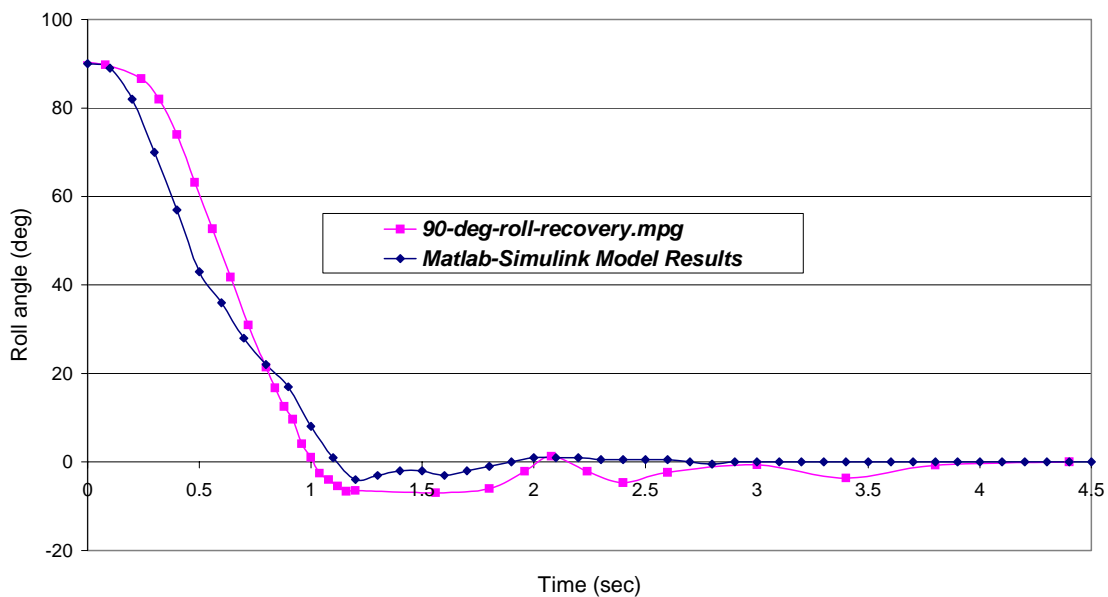


Figure 16: Experimental and simulated results show similar response rates and overshoot.

### Discussion

Actual flight-testing of the attitude stabilisation system has proven that the system does indeed function as intended. In some respects this work has been undertaken in reverse order, as the real system existed prior to this simulation project. Despite this, the simulation work provides two major outcomes. Firstly it verifies the process of operation based on independently sampled sensor data and shows similar behaviour to flight test results. Secondly, it can now serve as a tool to explore the limits of the autopilot functionality in terms of ‘acceptable performance’ for any given aircraft orientation and set of atmospheric conditions.

Based on the thermopile sensor data acquired, it appears that the autopilot performance would be degraded in situations of very low maximum temperature differential (MTD) between ground and sky. The errors created by non-uniform cloud cover or hot & cold patches on the ground are exacerbated in these situations. Despite this, the prototype system has flown successfully in hazy conditions where the MTD was only 3° C. Safe operation inside dense cloud or those with significant vertical movement is not expected due to the MTD being very low, with the temperature profile possibly becoming inverted in these instances.

That said, the systems performance in visual meteorological conditions (VMC) appears to be very good, even using only proportional control, as is currently the case on the test aircraft. The implementation of more sophisticated control algorithms may further improve the autopilot’s performance. This work is currently underway along with a revision of the analogue electronics, providing higher resolution and thus better performance in low MTD conditions.

During the project a tool was developed to allow batch runs of the same model but at various controller gain settings. This allows verification of the performance of the system at a given setting but also allows a trial and error approach to tuning the PID control loop. The figure below shows a series of system responses to varying controller gains. This scenario is a 90 degree roll recovery run using controller proportional gains from (10 to 60) \* $\pi/180$ .

### Conclusion

The functionality of the autopilot system based on thermopile sensors has been proven both theoretically and practically. The entire aircraft and autopilot system have been successfully modelled and verified utilising the Maple, Matlab and Simulink software tools [5,6]. The use of the ‘Aerosim’ Simulink block- set [7] was instrumental to the project, providing the six-degree of freedom aircraft model, to which all the additional systems could be grafted.

The work done is now at the stage where it could be used to test system performance under different gain settings for the PID controller or even entirely new control strategies to see their impact on the resulting aircraft behaviour.

The current system appears suited to its intended market - low-cost civilian UAV’s (unmanned aerial vehicles) where the mission often dictates operation in VMC conditions.

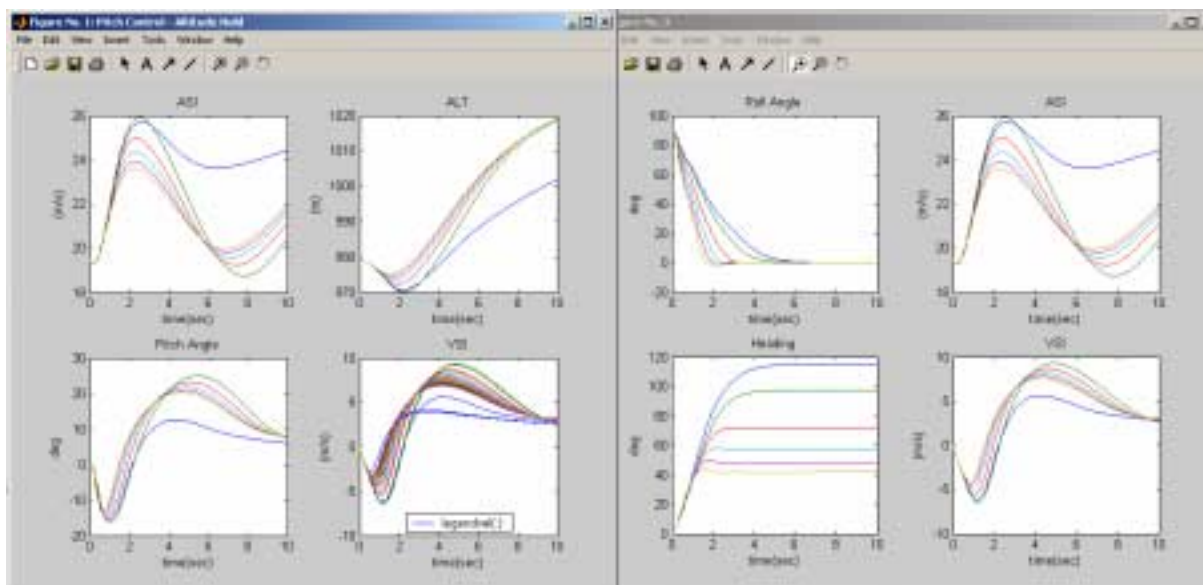


Figure 17: System response to varying control gains. 90 degree roll recovery with controller proportional gains from

### ***Suggested further work***

The aerodynamic derivatives currently being used are based on an aircraft with the same basic configuration that is geometrically similar. This is seen as a starting point only and further work either on empirical methods, CFD or actual aerodynamic wind tunnel testing would likely provide better results, improving the accuracy of the simulation.

Fitting the test aircraft with inertial sensors or other attitude referencing systems would allow a much more detailed and complete comparison with the simulation. The current comparison is based on captured video footage of a single manoeuvre.

### ***Acknowledgements***

This project was conducted with support from the Undergraduate Research Opportunity Program (UROP) and the School of Aerospace, Mechanical and Manufacturing Engineering at RMIT University.

The authors wish to thank the Monash University UAV Group for their involvement and assistance throughout the practical flight test phase and in particular Ray Cooper for volunteering his excellent piloting skills during the test flights.

### ***References***

1. Soule, Hartley, A., Miller, Marvel, P.: *The Experimental Determination of the Moments of Inertia of Airplanes*, NACA Rep. No. 467. 1933.
2. Kirschbaum, H.W.: *Estimation of Moments of Inertia of Airplanes from Design Data*, NACA TN No. 575, 1936.
3. *Understanding Thermopile Infrared Sensors*, W. Schmidt, Dr. J Schieferdecker  
Accessed 14/2/03  
<http://optoelectronics.perkinelmer.com/library/papers/tp6.htm>
4. *Melexis Datasheet for the MLX90247 thermopile sensor*, Accessed 14/2/03  
<http://www.melexis.com/prodmain.asp?search=thermopile&family=MLX90247>
5. *Maple V Release 4*, Waterloo Maple Inc, 1996
6. Matlab / Simulink Version 6.0.0.88 Release 12, *The MathWorks, Inc* ,© 1984-2000
7. *AeroSim aeronautical simulation blockset for Matlab*, Unmanned Dynamics, Accessed 30/02/03 <http://www.unmannedynamics.com/contact.htm>
8. Taylor, B., Bil, C., Watkins, S., Egan, G.: *Horizon Sensing Attitude Stabilisation: A VMC Autopilot*, 18<sup>th</sup> International UAV Systems Conference, Bristol, UK, 2003
9. Videopoint Version2.1, Lenox Softworks © 1999, <http://www.lsw.com/videopoint>